SLAC-PUB-9325
July 2002

FLUKA CALCULATIONS OF RADIONUCLIDES, STAR, AND NEUTRON FLUENCE IN SOIL AROUND HIGH-ENERGY ELECTRON AND PROTON LINEAR ACCELERATORS

Andrew Puryear

Texas A & M University
College Station, Texas 77841

James C. Liu and Sayed Rokni

Presented at the 6th Meeting on Shielding Aspects of Accelerators, Targets and Irradiation Facilities (SATIF6), 4/10/2002—4/12/2002, Menlo Park, CA, USA

Stanford Linear Accelerator Center, Stanford University, Stanford, CA 94309

Work supported by Department of Energy contract DE–AC03–76SF00515.

SLAC-PUB-9325 (April 2002)

FLUKA CALCULATIONS OF RADIONUCLIDES, STAR, AND NEUTRON FLUENCE IN SOIL AROUND HIGH-ENERGY ELECTRON AND PROTON LINEAR ACCELERATORS

Andrew Puryear (Texas A&M University, College Station, Texas 77841)
James C. Liu and Sayed Rokni (Stanford Linear Accelerator Center, California, 94025)

Abstract

Information of radionuclide production and the attenuation of high-energy neutrons in the soil shielding around accelerators is important for environmental impact assessment. The radionuclide concentration of ^{3}H, ^{7}Be, ^{22}Na, ^{24}Na, ^{45}Ca, ^{54}Mn, and ^{55}Fe in the soil outside the cylindrical concrete tunnel from a uniform beam loss along a copper Linac was calculated using FLUKA. The atom concentration and the number of atom per star for radionuclides were given as a function of soil depth. Attenuation length of star density, as well as the neutron fluence spectra, was calculated. Studies for electron and proton beams at 500 GeV were made and their results were compared to examine the common understanding that the radiation and radioactivity patterns outside a certain thickness of shielding are the same between high-energy electron and proton beams. The effects of star-scoring threshold (20 or 50 MeV) by neutrons or by all particles on the results were also investigated.

Introduction

To evaluate the environmental impact, the information of radionuclide yields and the attenuation of radiation (mainly the high-energy neutrons, which propagate the cascade) in the soil shielding around a high-energy accelerator is important. In this study, the atomic concentration of some important radionuclides (^{3}H, ^{7}Be, ^{22}Na, ^{24}Na, ^{45}Ca, ^{54}Mn, and ^{55}Fe) in the soil surrounding the cylindrical Linac tunnel was calculated using FLUKA [1,2] for the case of a uniform beam loss. The attenuation length of star density in soil and the neutron fluence spectra in soil were also calculated. The effects of scoring threshold (20 or 50 MeV) for star production on the results were investigated. Studies for a 500-GeV electron beam and a 500-GeV proton beam were made to examine the understanding [3] that the radiation and radioactivity patterns outside a certain thickness of shielding are the same between high-energy electron and proton machines.

FLUKA Calculations

A cylindrical geometry (see Figure 1), symmetric about the Z-axis, was used in FLUKA to simulate the concrete tunnel and the soil surrounding of a Linac. The origin was at the center of the tunnel front face. The concrete tunnel is coaxial with the Z-axis (inner radius 100 cm, outer radius 130 cm, a length of 1200 cm). The Linac is simulated as a copper rod (radius 2.5 cm and a length of 1200 cm) in the center of the concrete cylinder. Six layers of soil, each layer having a radial thickness of 30 cm, surround the concrete cylinder. All soil layers are divided into three sections along the Z-axis: the front section from 0 to 500 cm, the middle section from 500 to 1000 cm, and the back section from 1000 to 1200 cm. The main focus is in the middle section because it represents a “uniform” region for a line source, as shown below. Every soil region is numbered (1-18) for future reference.

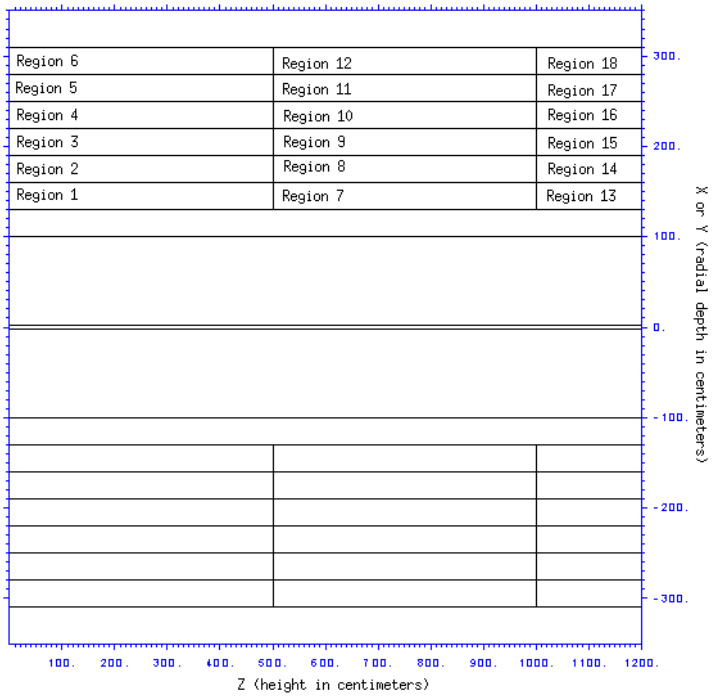

Figure 1. FLUKA cylindrical geometry for the Linac and tunnel.

The concrete had a density of 2.35 g/cm^3 with a composition (by weight) of O (50.0%), Ca (19.5%), C (3.0%), Al (3.0%), Fe (1.4%), Na (1.0%), K (1.0%), H (0.6%), and Mg (0.5%). The SLAC soil used in this study had a density of 2.1 g/cm^3 with a composition of O (54.6%), Si (30.7%), Al (4.2%), K (2.5%), Fe (1.8%), Mg (1.7%), H (1.6%), Na (1.3%), Ca (1.2%), Mn (0.003%) and the remaining fraction from B, Ti, V, Cr, Co, Ni, Cu, Zr, and Ba. Based on the hydrogen content of the SLAC soil, the water content of the SLAC soil is 29.4% by volume (14.2% by weight).

The new evaporation module was activated. All photonuclear reactions were activated in all materials. The interaction length of nuclear inelastic interactions of photons is biased by a factor of 50 in all materials to increase photoneutron production. Full leading particle biasing was activated for all electromagnetic processes in all regions. The region importance biasing for all particles is activated in the soil regions. Neutrons were transported down to thermal while other hadrons had a transport cut-off at 10 keV. The transport cut-off was 5 MeV for electrons, positrons, and photons. Muon was discarded.

Simulations were made for 500-GeV electron (250000x7 particles) and 500-GeV proton (5000x7 particles) beams with the star-scoring threshold at either 20 MeV (default) or 50 MeV. The beam particles hit the copper Linac uniformly between Z=0 to Z=1200 cm. The star density profiles (star/cm^3/beam particle) with the 50-MeV threshold for both the electron and proton beams were found to be constant within 6.4% in the first layer of soil for Z = 500 - 1000 cm. Thus, the FLUKA results in the middle section of soil regions (7-12) can be used for a line source situation.

The radionuclide of ^{3}H, ^{7}Be, ^{22}Na, ^{24}Na, ^{45}Ca, ^{54}Mn, and ^{55}Fe were scored directly in soil regions 7-12 using the RESNUCLE card and the results were post-processed using the program rusrsuw. The star densities produced by neutrons and by all particles (hereafter called neutron star and all star, respectively) in the soil regions were scored using SCORE. The atom/star values were then calculated using the radionuclide concentration and star density values. The spatial distributions of neutron star density and all star density in regions 7-12 were scored using USRBIN for radius from 130 to 310 cm (12 bins) and for Z from 500 to 1000 cm (25 bins). Attenuation lengths of star in soil were calculated based on the star profiles. Finally, the neutron fluence spectra were scored in regions 7-12 using the USRTRACK card.

Results

Figure 2a (electron beam) and Figure 2b (proton beam) show the atom concentration of each radionuclide as it varies radially for regions 7-12. There appears to be 2 distinct slopes for ^{24}Na, ^{45}Ca, and ^{55}Fe (in particular, for the electron beam case), while the rest has only one slope. The star density

(dominated by neutron star at all depths) decreases radially, resembling the pattern of most radionuclides. The neutron star density approaches the all star density in outer soil regions meaning that, in deep soil, neutron will eventually become the only contributing particle to stars. This can also be clearly seen in Figure 3.

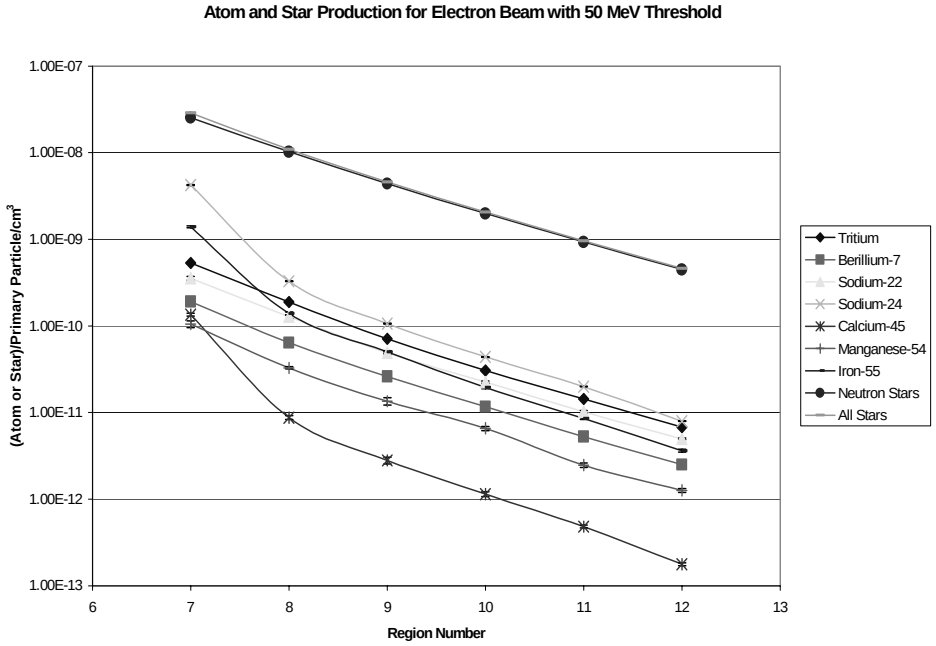

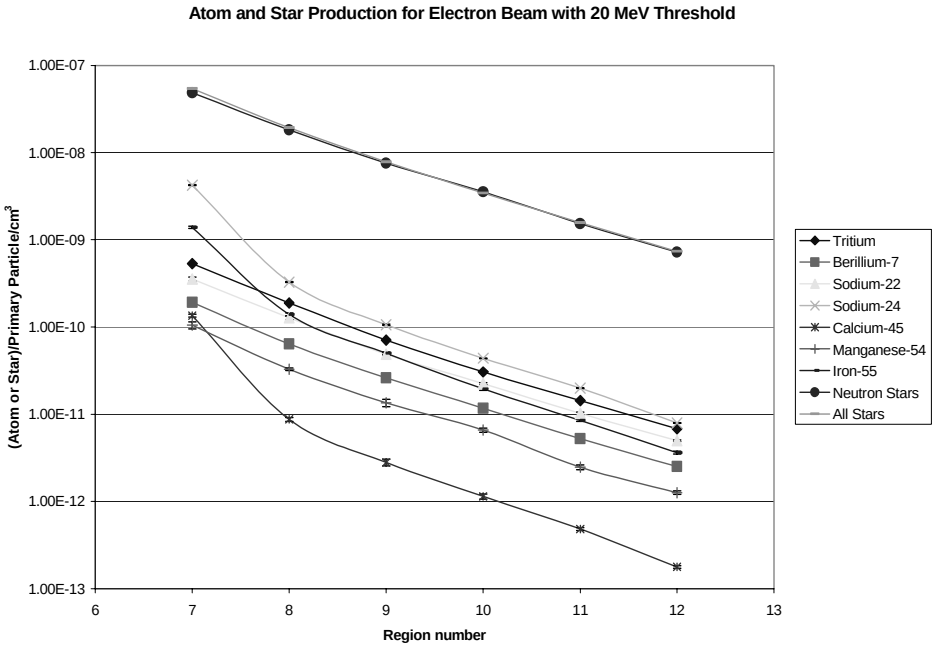

Figure 2a. Radionuclide concentration and star density in soil regions 7-12 for electron beam with 50 (top) and 20 MeV (bottom) star-scoring thresholds.

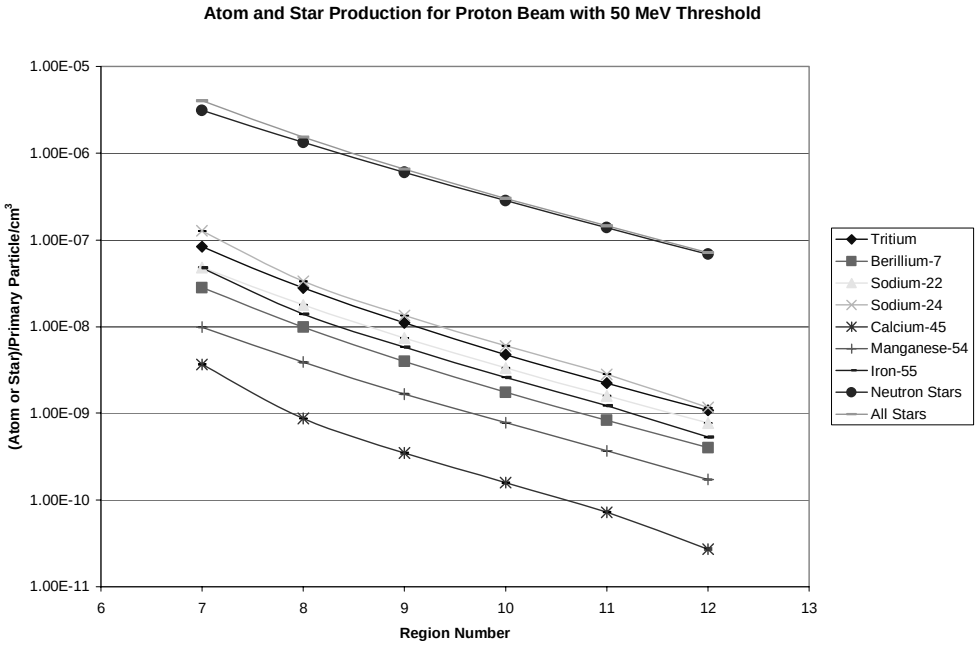

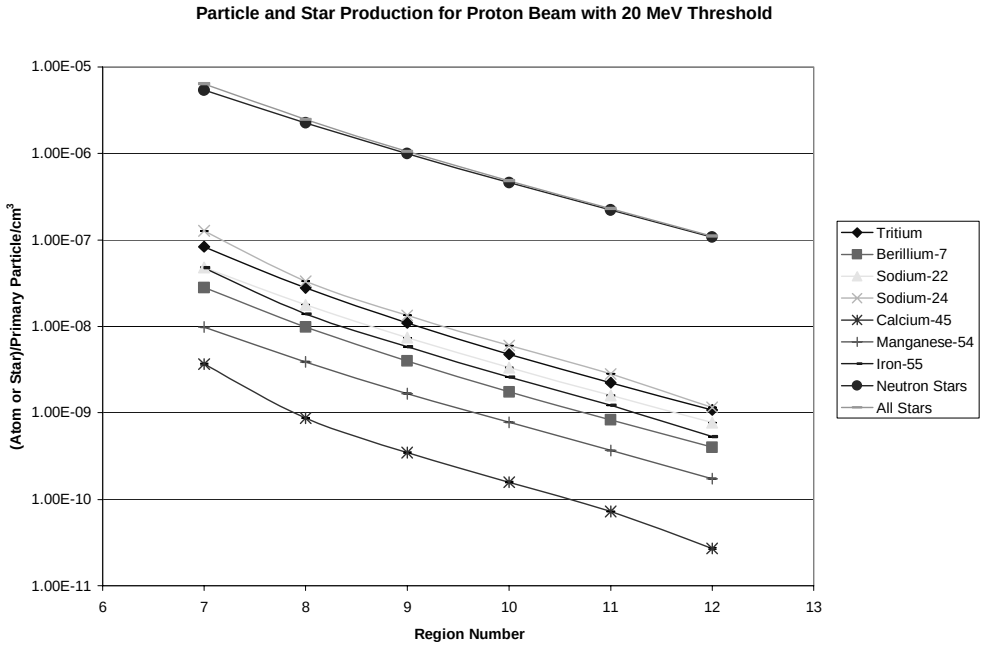

Figure 2b. Radionuclide concentration and star density in soil regions 7-12 for proton beam with 50 (top) and 20 MeV (bottom) star-scoring thresholds.

The star profiles in soil regions for electron and proton beams with 50 and 20 MeV star-scoring thresholds are summarized in Figure 3 (left). Proton beam produces a star density that is a factor of 123-153 higher than the corresponding case of electron beam. The ratios of star density, normalized to the all star density with 50-MeV threshold, for either the electron or proton beam are shown in Figure 3 (right). In any case, the neutron star density is over 80% of the all star density at all depths. The star density for 20-MeV threshold is ~1.5 times higher than that for 50-MeV threshold. It is clear that, at region 11 (i.e., 30-cm concrete plus 120-cm soil ≈ 150-cm soil), the "equilibrium" state was reached. Note that the equilibrium state is reached earlier for electron beam than for proton beam and also earlier for 50-MeV than for 20-MeV threshold.

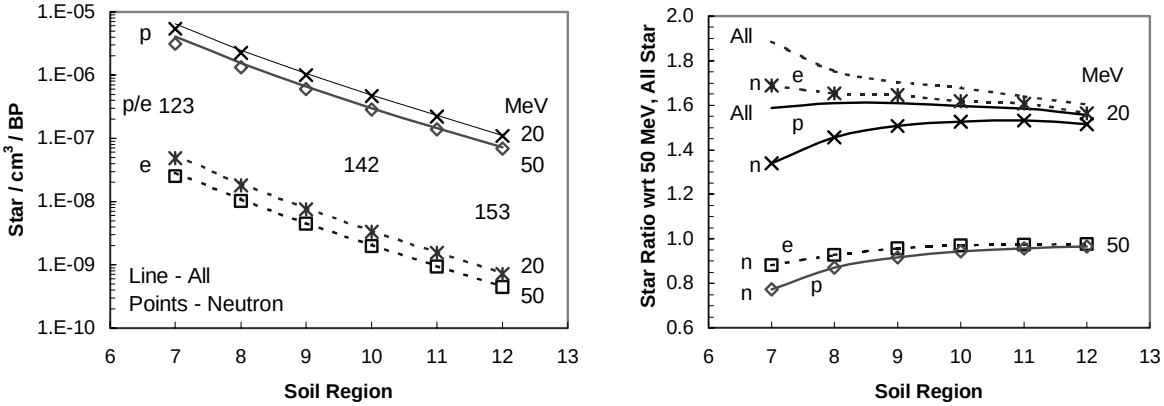

Figure 3. Comparison of star density profiles in soil regions 7-12 between electron and proton beams and with 50 and 20 MeV star-scoring thresholds (left) and the ratio of star density when normalized to the all star density with the 50-MeV threshold (right).

Dividing the radionuclide concentration by the all star density in the same soil region, Figure 4 was obtained. For most radionuclides, the results of atom per star are different for electron and proton beams within region 8 (< 90 cm soil). However, the atoms per star are similar beyond region 9 (> 120 cm soil). At these equilibrium depths, a number of 0.01 atoms per all star can be used for the estimations of the yield for most radionuclides (within a factor of 3), except for ^{54}Mn and ^{45}Ca.

Using ^{3}H as an example, a close examination of the charactersitcis of the atom per star profiles is given in Figure 5. Again, electron and proton beams have different atom/star values within shallow regions, but the difference is < 10% beyond region 9. Note that the difference between electron and proton beams is smaller in the case of atom per all star. This is likely due to the fact that proton beam produces many types of hadrons while electron beam produces mainly neutrons. Proton beam has high atom/star values than electron beam. However, at deep regions, the atom per star approaches an asymptotic value (0.015 ^{3}H/star at 50-MeV threshold and 0.01 ^{3}H/star at 20-MeV threshold), which is independent of beam type as well as the type of star (all star or neutron star). This indicates that neutrons are the only particles that produce stars and radionuclides at deep regions. Again, the equilibrium state was reached at region 10 (> 120 cm soil) for electron beam and region 11 (> 150 cm soil) for proton beam.

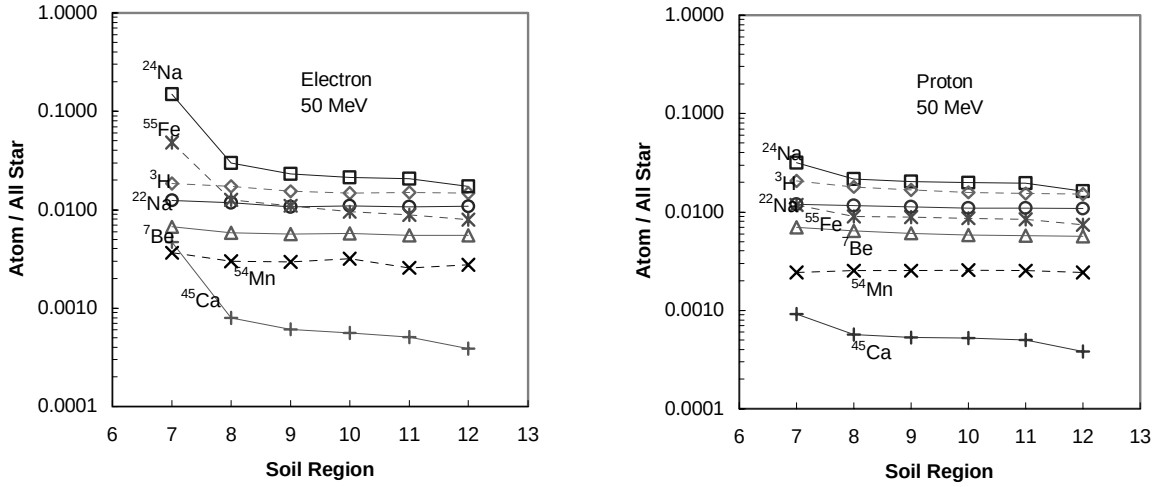

Figure 4. Number of radionuclide per all star in soil regions 7-12 for electron and proton beams with 50-MeV star-scoring threshold.

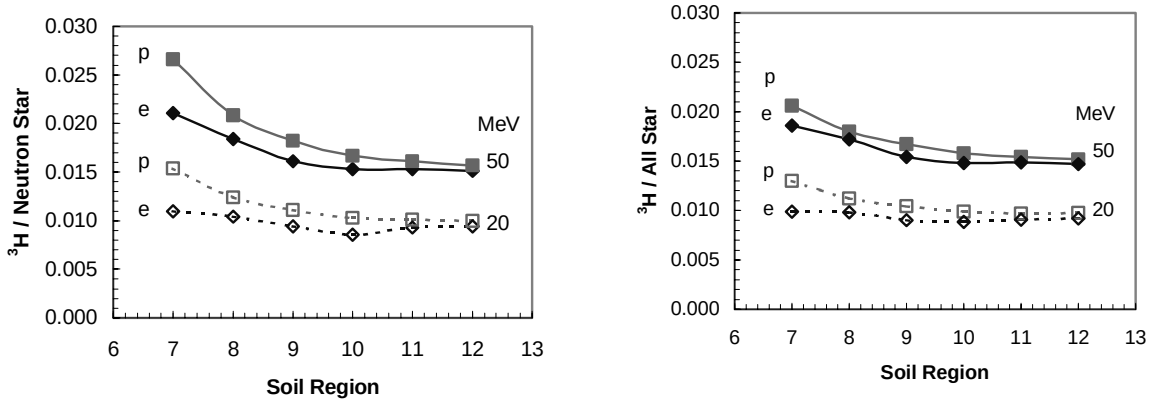

Figure 5. Number of ^{3}H atom per neutron star (left) and per all star (right) in soil regions 7-12 for electron and proton beams with 20 MeV and 50 MeV star-scoring thresholds.

The attenuation length of all star density in soil was obtained from its profile as a function of radius in the soil. The all star density is plotted in Figure 6 as a function of radius (130 to 310 cm) at Z=800 cm. It appears that, beyond radius r = 220 cm (i.e., beyond region 9), the slopes become constant. Thus, after corrected with 1/r for the line source geometry, attenuation lengths can be calculated by performing a least square exponential fit to the last 5 points of the curves (the equilibrium part) in Figure 6. The calculated attenuation length at equilibrium depth ranges from 97 g/cm^2 (for electron beam with 20-MeV threshold) to 105 g/cm^2 (for proton beam with 50-MeV threshold). The attenuation length for proton beam is higher (~4%) than that of electron beam, and the attenuation length at 50-MeV threshold is also 4% higher than that at 20-MeV threshold. The errors associated with attenuation lengths were < 2%, estimated using different number of points in fitting.

It is known [4,5] that the attenuation length varies as a function of angle; the larger the angle, the smaller the attenuation length. Fasso [4] found that, for GeV electron beams, the attenuation length varied from 73 gm/cm^2 at 90^o to 125 gm/cm^2 at 30^o, and he recommended a conservative value of 100 g/cm^2 for the lateral shield of high-energy electron accelerators. Dinter [5] found similar dependence with 95 gm/cm^2 at 90^o to 110 gm/cm^2 at 30^o for electron beam, as well as 110 gm/cm^2 at 90^o to 140 gm/cm^2 at 30^o for proton beam. The attenuation length results (at equilibrium depth for a line source) in this study are consistent with others (at any depth for a point source) [4,5]

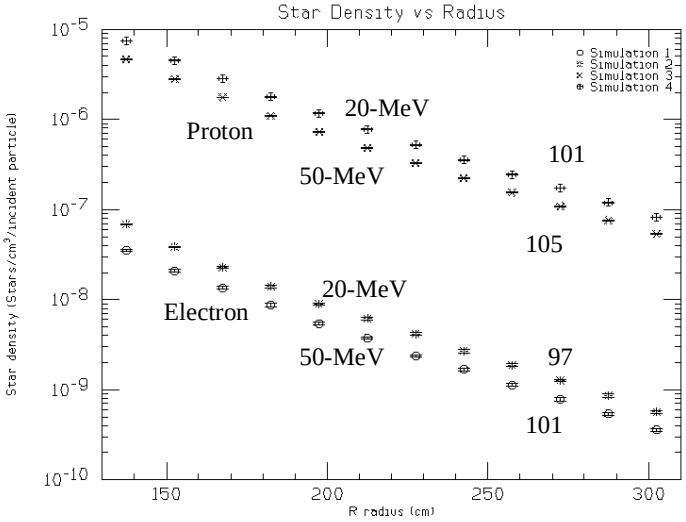

Figure 6. The all star density as a function of radius (130 to 310 cm) at Z=800 cm for electron and proton beam with 50-MeV and 20-MeV thresholds. The numbers shown on the right are attenuation lengths in soil (g/cm^2), calculated using the last 5 points of the curve.

The neutron fluence spectra in soil regions can provide insight and support conclusions for radionuclide production, as well as radionuclide per star. The neutron spectra in soil regions 7-12 are shown in Figure 7 for electron beam (top) and proton (bottom) beam. Both plots are lethargy plots of neutron fluence (neutron/cm^2/beam particle) vs. neutron energy (GeV). The two-peak feature (one at 1-2 MeV and the other at 100 MeV) is clearly seen. At shallow regions, the ratio between low-energy peak to high-energy peak is higher for electron beam than for proton beam. At deep regions, the spectral shapes for electron and proton beams are similar. Actually, beyond region 10, the spectrum reaches the equilibrium state for both electron and proton beams, and the neutron spectrum of proton beam is a factor of ~135 higher than that of electron beam.

Conclusions

The accurate prediction of induced radioactivity using FLUKA or another Monte Carlo codes is not at a perfect stage yet and a factor of 2-3 agreement is common for most radionuclides [6,7]. Thus, the absolute radionuclide yields in this study should not be paid special emphasis. The relative results between the electron and proton beams, between 50-MeV and 20-MeV star-scoring thresholds, or between neutron star and all star are of more interests, particularly at the equilibrium depth.

There are several main conclusions from this study:

1) As expected, the radionuclide profiles in the soil resemble the star profile beyond the shallow layer, which forms the basis of estimating the induced radioactivity using the star density.
2) Neutrons dominate the star production (> 80% at all depths). At deep regions, the star and radionuclide production is due to almost entirely by neutrons, with all other particles contributing to less than a few percent of the all star density.
3) Equilibrium state was reached beyond 120-cm-thick soil for electron and 150 cm for proton beam.
4) The atom/star factors for radionuclides are comparable for electron and proton beams, particularly at equilibrium depth. At equilibrium, a value of 0.01 atom/star can be used to estimate the yields of five radionuclides in this study for both electron and proton beams within a factor of 3.
5) At equilibrium, the attenuation length λ of star (contributed by neutrons only) is 100 g/cm^2, with λ for proton beam being 4% higher than λ for electron beam.
6) At equilibrium, the star density ratio between proton and electron beams is ~150, while the corresponding neutron fluence ratio is 135 (the spectral shape is the same). The star density at 20-MeV threshold is 1.5 times more than that at 50-MeV threshold.

.

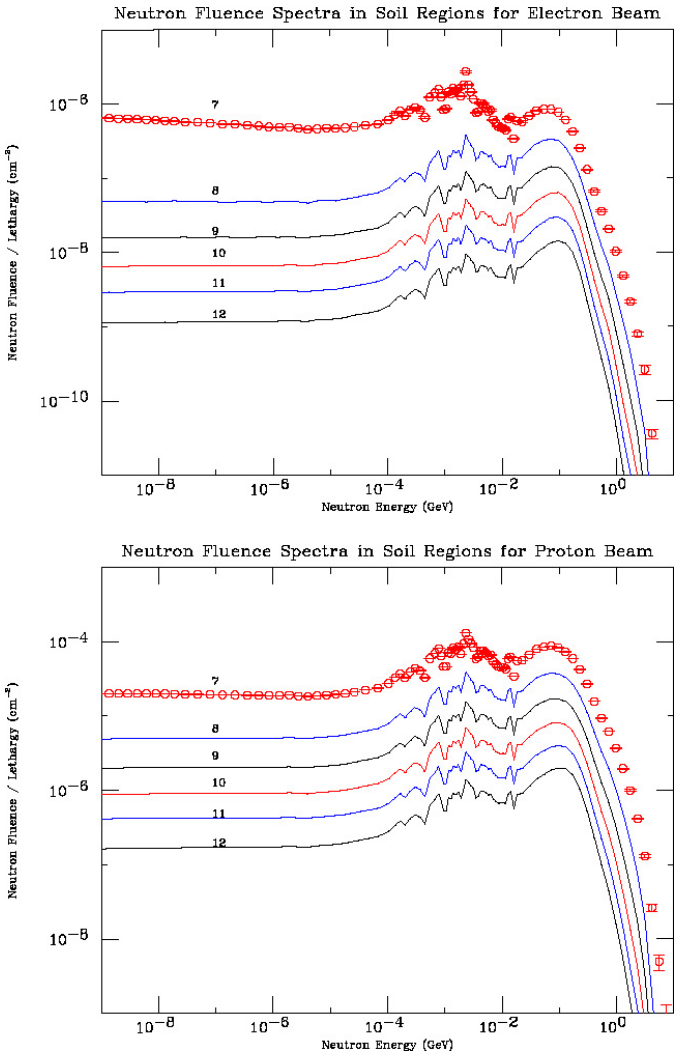

Figure 7. Neutron spectra (in lethargy plot per unit beam particle) in soil regions 7-12 for electron beam (top) and proton (bottom) beams.

Acknowledgements

The authors wish to acknowledge Alberto Fasso, Ralph Nelson, and Stefan Roesler for their help on this work. The work was supported by Department of Energy contract DE-AC03-76SF00515.

References

[1] A. Fasso, A. Ferrari, and P.R. Sala, "Electron-photon transport in FLUKA: status", Invited talk in the Proceedings of the Monte Carlo 2000 Conference, Lisbon, October 23-26 2000, A. Kling, F. Barao, M. Nakagawa, L. Tavora, P. Vaz eds., Springer-Verlag Berlin, p. 159-164, 2001.

[2] A. Fasso, A. Ferrari, J. Ranft, and P.R. Sala, "FLUKA: status and prospective for hadronic applications", Invited talk in the Proceedings of the Monte Carlo 2000 Conference, Lisbon, October 23-26 2000, A. Kling, F. Barao, M. Nakagawa, L. Tavora, P. Vaz eds., Springer-Verlag Berlin, p. 955-960, 2001.

[3] W. R. Nelson and T. M. Jenkins, "Similarities among the radiation fields at different types of high-energy accelerators", IEEE Transactions on Nuclear Science, NS-23, No. 4, August 1976.

[4] A. Fasso, M Hofert, and A. Ioannidou, "On the shielding of electron accelerators in the GeV energy range", Radiat. Prot. Dosim. 38(4), pp301-305, 1991.

[5] H. Dinter, A. Leuschner, K. Tesch, D. Dworak, and J. Loskiewicz, "Calculations of hadron yields around thick targets and doses behind concrete shielding of high-energy electron accelerators", Nucl. Instru. And Methods in Phys. Res. A455, p460-469, 2000.

[6] A. Fasso, M. Silari, and L. Ulrici, "Predicting induced radioactivity at high-energy electron accelerators", Preceedings of the 9th Internatinal Conference on Radiation Shielding, ICRS-9 Tsukuba, Japan, 1999, Nucl. Sci. Tech. 1 (Suppl.), p.827, 2000.

[7] S.H. Rokni, J.C. Liu, and S. Roesler, "Induced radioactivity of materials by stray radiation fields at an electron accelerator", this Proceedings.